Analysis of inelastic x-ray scattering spectra of low-temperature water

C. Y. Liao,[1] S. H. Chen,[1] and F. Sette[2]
[1]*Department of Nuclear Engineering, Massachusetts Institute of Technology, Cambridge, Massachusetts 02139*
[2]*European Synchrotron Radiation Facility, Boîte Postale 220, F-38043 Grenoble Cedex, France*
(Received 10 September 1999)

We analyze a set of high-resolution inelastic x-ray scattering (IXS) spectra from H_2O measured at $T=259$, 273, and 294 K using two different phenomenological models. Model I, called the ''dynamic cage model,'' combines the short time in-cage dynamics described by a generalized Enskog kinetic theory with a long-time cage relaxation dynamics described by an alpha relaxation. This model is appropriate for supercooled water where the cage effect is dominant and the existence of an alpha relaxation is evident from molecular-dynamics (MD) simulation data of extended simple point charge (SPC/E) model water. Model II is essentially a generalized hydrodynamic theory called the ''three effective eigenmode theory'' by de Schepper *et al.* [1]. This model is appropriate for normal liquid water where the cage effect is less prominent and there is no evidence of the alpha relaxation from the MD data. We use the model I to analyze IXS data at $T=259$ K (supercooled water). We successfully extract the Debye-Waller factor, the cage relaxation time from the long-time dynamics, and the dispersion relation of high-frequency sound from the short time dynamics. We then use the model II to analyze IXS data at all three temperatures, from which we are able to extract the relaxation rate of the central mode and the damping of the sound mode as well as the dispersion relation for the high-frequency sound. It turns out that the dispersion relations extracted from the two models at their respective temperatures agree with each other giving the high-frequency sound speed of 2900 ± 300 m/s. This is to be compared with a slightly higher value reported previously, 3200 ± 320 m/s, by analyzing similar IXS data with a phenomenological-damped harmonic oscillator model [2]. This latter model has traditionally been used exclusively for the analysis of inelastic scattering spectra of water. The *k*-dependent sound damping and central mode relaxation rate extracted from our model analyses are compared with the known values in the hydrodynamic limit.

PACS number(s): 61.20.Ja, 64.70.Pf

I. INTRODUCTION

Stimulated by a pioneering molecular-dynamic (MD) simulation made in 1974, which predicted the existence of a high-frequency propagating sound [3] in water, and a subsequent experimental verification of it by an inelastic neutron scattering (INS) spectroscopy [4] in 1985, the physical origin of the high-frequency sound in water has since been discussed extensively in the literature using MD simulation data [5,6] and by a further INS experiment of water [7]. However, because of the kinematic restriction in inelastic neutron spectroscopy and the different interaction potential models used in various MD simulations, the high frequency sound dispersion relation of water remains a controversial topic. Recently, a high-resolution inelastic x-ray scattering (IXS) technique has been developed, which can investigate a much larger (k,ω) region of the dynamic structure factor, $S(k,\omega)$, of the collective center of mass motion of water. Using this new tool, Sette *et al.* [8–10] found the transition of sound velocity from the low frequency adiabatic value, $c_0=1500$ m/s at low *k*, to a high-frequency value, more than twice larger, $c_\infty=3200\pm320$ m/s, at *k* value around 2 nm^{-1}. This transition was found to be temperature dependent and is probably related to the structural relaxation process in the connected region of hydrogen bond network in water [4,2]. To have a clear picture about the relation between the structural relaxation and *k*-dependent sound propagation, the specific models are needed to extract reliable values of the parameters governing the relaxation process and the sound propagation.

So far, these coherent INS and IXS data have been analyzed by assuming that the dynamic structure factor $S(k,\omega)$, expressing the power spectral density of the density fluctuation of the center of mass, consists of a central Lorentzian peak and two symmetrically energy shifted side peaks represented by the spectral density of a damped harmonic oscillator [4,8]. This latter line shape, chosen arbitrarily, nevertheless is routinely used to extract the basic features expected for the inelastic part of $S(k,\omega)$. From a purely experimental point of view, one usually observes a prominent central peak and two weak side wings from which one merely tries to extract, phenomenologically, the position and width of the side peaks. From *k* dependence of these two quantities, one then extracts the propagating high-frequency sound speed and the *k*-dependent damping constant of the sound. One should keep in mind, however, that the above mentioned conventional way of the spectral analysis ignores the intimate (theoretical) connection between the spectral intensities of the three lines and assumes the existence of the two side peaks with an arbitrary proportion of intensities with respect to the central line. This results in too many parameters in the fitting function (four). At present, INS is a rather difficult experiment to do, which requires deuterated liquids and state-of-the-art neutron instruments available only at few places in the world. The high-resolution IXS spectrometer, on the other hand, is a brand new development existing only at a third generation synchrotron x-ray source at the Euro-

pean Synchrotron Research Facility (ESRF) in Grenoble, France. One therefore would like to have a theory which is applicable for describing large k density fluctuations that gives the relative intensities of the triplet and thereby can extract from the measured spectra more information with regard to the molecular scale density fluctuation in an important fluid like water. This paper is a first step toward this goal by presenting two phenomenological models for the analysis of existing high-resolution IXS data for the low- and high-temperature water.

The IXS experiment was carried out at a very high-resolution inelastic x-ray scattering beam line (BL21-ID 16) at the ESRF. The undulator x-ray source was monochromated by a Si(111) double crystal monochromator and a high-energy resolution back scattering monochromator (temperature controlled and scanned), operating either at the Si(999) (x-ray energy 17.794 KeV) or Si(11 11 11) (21.748 KeV) Bragg reflections. The scattered photons were collected by a grooved spherical silicon crystal analyzer operating at the same Bragg backreflections, and in Rowland geometry. The net energy resolution function was measured by an elastic scattering of a plastic sample at its maximum of the structure factor. The energy resolutions were 3.2 and 1.5 meV (full width at half maximum [FWHM]) for Si(999) and Si(11 11 11) reflections respectively. The x-ray beam size at the sample was 0.1 mm×0.3 mm and the high-purity water sample thickness was 18 nm [11]. The IXS measurements on H_2O were made at k-values of 1, 2, 4, 7, 10 nm^{-1} at two temperatures $T=294$, 273 K, and at k values of 2, 4, 6, 8, 10 nm^{-1} at a temperature $T=259$ K. To maintain the density of $\rho\sim 1.0\ g/cm^3$ at a supercooled temperature, a pressure of $P=2.0$ kbar was applied to the sample at $T=259$ K [2].

II. DYNAMIC CAGE MODEL

The dynamic cage model has been developed to analyze the collective part of intermediate scattering function (ISF) generated from MD data of extended simple point charge (SPC/E) supercooled water [12]. It combines the short time in-cage dynamics described by a generalized Enskog kinetic theory with a long-time cage relaxation dynamics described by an alpha relaxation. The latter is appropriate when the cage effect is dominant and the ISF shows a well separated two-step relaxation. According to a previous MD simulation [13], ISF of supercooled water initially decays within 1 ps to a plateau value determined by a coherent Debye-Waller factor. Then it relaxes slowly, according to a stretched exponential time dependence, with a k-dependent relaxation time τ and a stretch exponent β (see Fig. 1). The evolution of ISF can therefore be expressed as a product of two factors: the relaxation function representing motions within the cage and the cage relaxation function. The in-cage relaxation function decays from an initial value of unity to the Debye-Waller factor at long-time defined by the potential well of the confining cage. The cage relaxation caused by the local structural relaxation can be described by an α relaxation described by the well-known Kohlrausch form $\exp[-(t/\tau)^{\beta}]$. The ISF for the entire time range is therefore written as

$$\frac{F(k,t)}{S(k)}=\{[1-A(k)]F_{\mathrm{QTRT}}(k,t)+A(k)\}\exp\left[-\left(\frac{t}{\tau}\right)^{\beta}\right], \tag{1}$$

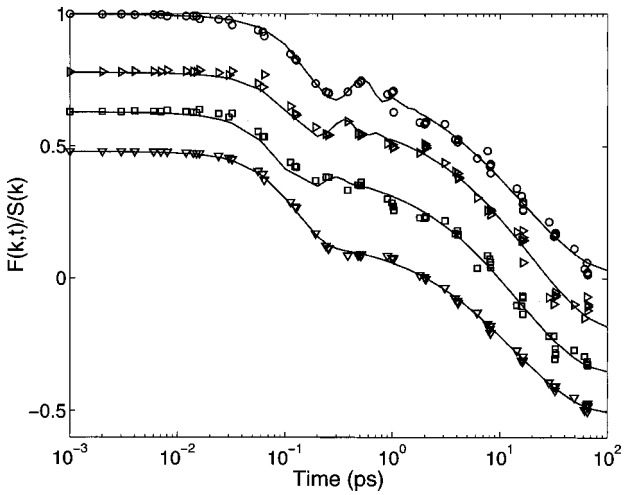

FIG. 1. A set of MD simulation generated intermediate scattering functions, $F(k,t)/S(k)$, of the center of mass of water at $T=238$ K at different k values: $k=3.3\ nm^{-1}$ (circle), 4.4 nm^{-1} (right triangle), 6.7 nm^{-1} (square), 22.3 nm^{-1} (down triangle). The solid lines are fits by the dynamic cage model. The values of structure factor $S(k)$ are taken from the SPC/E MD simulation at the same temperature.

where $A(k)$ is the coherent Debye-Waller factor and $F_{\mathrm{QTRT}}(k,t)$ the normalized ISF calculated by a modified Q-dependent triple relaxation time (QTRT) kinetic model [12]. The conventional QTRT [14,15] is an approximate solution of the generalized Enskog equation which calculates the dynamic structure factor $S(k,\omega)$ from a given structure factor $S(k)$. The calculated dynamic structure factor has the correct third moment for the hard sphere system [12] as well as the correct second moment for general fluids. The conventional QTRT gives the correct form for the two well-understood limiting cases: for dilute gasses and dense fluids in the hydrodynamic regime. Furthermore, it has an appropriate analytical structure that describes a continuous transition between these two limits [15], and is known to describe the density fluctuation of moderately dense hard sphere fluids well [16,17]. The conventional QTRT has three input parameters, aside from the well-known thermodynamic parameters (such as thermal speed v_0): the static structure factor $S(k)$, the pair correlation function at contact $g(\sigma)$, and the hard sphere diameter σ. Since the generalized Enskog kinetic equation considers only uncorrelated binary collisions between hard spheres, one need an additional correlated collision term to describe the dense fluids at larger wave vectors probed by the IXS. In Ref. [12], we showed schematically that for supercooled water where the local structural relaxation time is well separated from the in-cage relaxation time, the interplay of the binary collision term and the correlated collision term at the memory function level leads to the de-coupling form of ISF as given by Eq. (1). To give the correct second and third frequency moment of the spectrum corresponding to ISF in Eq. (1), one has to multiply the thermal speed $v_0=(k_BT/m)^{1/2}$ by a factor $1/[1-A(k)]^{1/2}$ and the $g(\sigma)$ by a factor $[1-A(k)]^{1/2}$ [12]. This modification shows that the Debye-Waller factor, describing the cage formation at different wave vector, has a significant effect on the in-cage short-time (high frequency) dynamics. The Eq. (1) and its corresponding modification of the con-

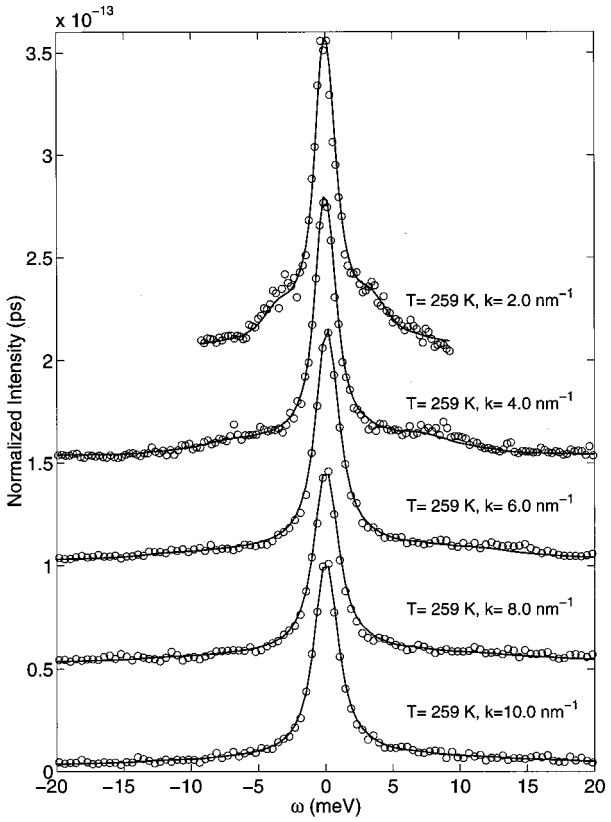

FIG. 2. IXS spectra of H_2O at $T=259$ K taken at the indicated k values. The experimental data are shown together with the fits (solid line) by the dynamic cage model as explained in the text. The experimental data is normalized to have unity area over the measured energy transfer range.

ventional QTRT has been shown to be essential in fitting the MD generated ISF of supercooled water [12].

In order to fit IXS data, Eq. (1) is Fourier transformed to obtain the dynamic structure factor, multiplying by the detailed balance factor, and convoluted with the energy resolution function $R(\omega)$.

$$S(k,\omega)/S(k)=[1-A(k)]S_{\mathrm{QTRT}}(k,\omega)\otimes S_{s\ \exp}(k,\omega)\otimes R(\omega)+A(k)S_{s\ \exp}(\omega)\otimes R(\omega), \qquad (2)$$

where $S_{\mathrm{QTRT}}(k,\omega)$ is the dynamic structure factor calculated by the modified QTRT kinetic model, and $S_{s\ \exp}(k,\omega)$ the Fourier transform of the stretched exponential. We fitted the lowest temperature ($T=259$ K) IXS data of water using Eq. (2). The IXS spectra at $T=259$ K, taken at different wave vector k, are shown in Fig. 2. together with the model fits. At both sides of the quasi elastic line, it is apparent that there are inelastic scattered intensity at energies that change with k. These inelastic scatterings are due to collective excitations in water [18].

Since the IXS spectra of water at supercooled temperature were taken at a pressure of 2.0 kbar, there is no experimental center-of-mass structure factor available at this condition. We therefore use the value of the static structure factor $S(k)$ from a MD simulation at temperature $T=270$ K [5]. The structure factor as shown in Fig. 5 in the low-k region is rather flat, and the temperature variation is weak in this k region (see Fig. 2 in Ref. [5]). In the fitting, the stretch exponent β is fixed at a value 0.75 (from MD), the hard sphere diameter $\sigma=27.5$ nm and $g(\sigma)=3.2$ [12]. Therefore, there are only two adjustable parameters: the k-dependent cage relaxation time $\tau(k)$ and the Debye-Waller factor $A(k)$, which are listed in Table I. The individual contributions of the QTRT versus the stretched exponential in a typical fit ($k=4$ nm^{-1}) are shown separately in Fig. 3. The total fit curve is the sum of the two types of contributions. The QTRT contribution is the convolution of the spectrum calculated by modified QTRT method with the spectrum of the stretched exponential, since the spectrum of the stretched exponential is a very sharp curve, the convoluted QTRT contribution remains a similar shape as the original one. The inset of Fig. 3 shows that the stretched exponential contributes mainly to the quasi elastic central line, and the QTRT contributes to the high frequency excitations. One may note that the use of a stretched exponential to model a quasi elastic central line has been reported in the Ref. [18] where the authors analyzed the high-resolution quasielastic incoherent neutron scattering of supercooled water contained in a porous glass. The dynamic cage model is seen to successfully separates contribution of the inelastic spectrum, modeled by the modified QTRT, from that of the quasi elastic central line, modeled by the stretched exponential.

TABLE I. The extracted parameters by fitting IXS data at $T=259$ K with the dynamic cage model.

k (nm^{-1})	2.0	4.0	6.0	8.0	10.0
$A(k)$	0.625	0.719	0.765	0.773	0.780
$\tau(k)$ (ps)	2.88	2.24	1.11	1.14	1.18

III. THREE EFFECTIVE EIGENMODE (TEE) MODEL

The TEE model has already met with successes in describing the behavior of dynamic structure factor at finite k

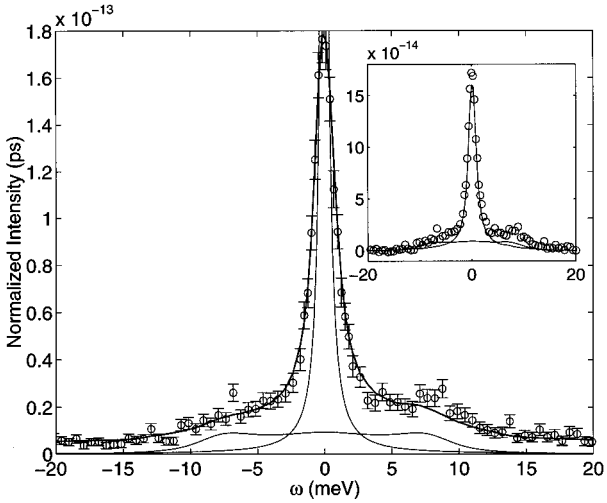

FIG. 3. IXS spectra of H_2O at $T=259$ K, $k=4$ nm^{-1} (open circle) shown together with the fit with the dynamic cage model (thick solid line), the QTRT and stretched exponential contribution before convolution with the resolution function. The inset is the QTRT and stretched exponential contribution after convolution with the resolution function.

values for hard sphere system [19–21], Lennard-Jones fluids [1], classical fluids like Ar, Ne, Kr, ^{4}He at high temperature, and super fluid ^{4}He [22]. For these cases it has been shown that ISF of the density fluctuation can be well described by a sum of three exponential functions associated with three slow conserved hydrodynamic eigenmodes of the fluid, the so-called extended heat mode and two extended sound modes. Although this description is an extended hydrodynamic model, it has been shown that it provides a good approximation for the $S(k,\omega)$ in the wide-k range from 0 up to $15k\sigma_{LJ}$ [1], where σ_{LJ} is Lennard-Jones diameter. The TEE model can be derived from Zwanzig-Mori projection operator formalism [23,24], in Appendix we give another plausible argument for the TEE model. In the TEE model, the correlation function matrix $\vec{\vec{G}}(k,z)$ for the three slow microscopic fluctuations: number density (labeled as ''n''), longitudinal velocity (labeled as ''u''), and energy (labeled as ''T''), obeys a hydrodynamic-like equation:

$$z\vec{\vec{G}}(k,z) = -\vec{\vec{H}}(k)\vec{\vec{G}}(k,z) + \vec{\vec{I}}, \tag{3}$$

The dynamic structure factor is then given as,

$$S(k,\omega) = \frac{S(k)}{\pi}\mathrm{Re}\left\{\frac{\vec{\vec{I}}}{i\omega\vec{\vec{I}} + \vec{\vec{H}}(k)}\right\}_{1,1}, \tag{4}$$

where $\vec{\vec{I}}$ is the 3×3 identity matrix, label 1,1 means the (1,1) element of the matrix. The matrix $\vec{\vec{H}}(k)$ is

$$\vec{\vec{H}}(k) = \begin{pmatrix} 0 & if_{un}(k) & 0 \\ if_{un}(k) & z_u(k) & if_{uT}(k) \\ 0 & if_{uT}(k) & z_T(k) \end{pmatrix}, \tag{5}$$

with $f_{un}(k)$ determined by the second moment of $S(k,\omega)$ to be $kv_0[S(k)]^{1/2}$. Three independent parameters: $z_u(k)$, $f_{uT}(k)$, $z_T(k)$ are all real numbers. For small k, the Eq. (5) tends to the hydrodynamic matrix where the matrix elements have values given by [1,25]:

$$f_{un}(k) = kc_s/\sqrt{\gamma} \tag{6a}$$

$$z_u(k) = \phi k^2 \tag{6b}$$

$$z_T(k) = \gamma D_T k^2 \tag{6c}$$

$$f_{uT}(k) = kc_s\sqrt{(\gamma-1)/\gamma}. \tag{6d}$$

Here, $c_s = v_0[\gamma/S(0)]^{1/2}$ is the adiabatic speed of sound; $\gamma = c_p/c_v$ is the ratio of the specific heat per unit mass at constant pressure and volume; $\phi = [(4/3)\eta + \zeta]/\mathrm{nm}$ is the kinematic longitudinal viscosity, where η and ζ are the shear and bulk viscosity, respectively; $D_T = \lambda/\mathrm{nmc}_p$ is the thermal diffusivity, where λ is the thermal conductivity. The three eigenvalues of the hydrodynamic matrix are therefore the three hydrodynamic modes. Here, we only give the three eigenvalues up to the order of $O(k^2)$

$$z_h(k) = D_T k^2 \quad \text{(heat mode)} \tag{7a}$$

$$z_{\pm}(k) = \pm ic_s k + \Gamma_s k^2 \quad \text{(sound mode)}, \tag{7b}$$

where $\Gamma_s = (1/2)\phi + (1/2)(\gamma-1)D_T$ is the sound damping.

For finite k, $z_u(k)$, $f_{uT}(k)$, $z_T(k)$ become arbitrary functions of k. However, in most cases, the eigenvalues of the matrix [Eq. (5)] consists of one real number z_h and a couple of conjugate complex numbers $\Gamma_s \pm i\omega_s$. We can therefore write the solution of Eq. (5) in general in the hydrodynamiclike form [15,26].

$$S(k,\omega)/S(k) = \frac{1}{\pi}\left\{A_0\frac{z_h}{\omega^2+z_h^2} + A_s\frac{\Gamma_s + b(\omega+\omega_s)}{(\omega+\omega_s)^2+\Gamma_s^2} + A_s\frac{\Gamma_s - b(\omega-\omega_s)}{(\omega-\omega_s)^2+\Gamma_s^2}\right\}. \tag{8}$$

The correlation function of the density fluctuation is the corresponding time-domain result [27]:

$$F(k,t)/S(k) = A_0\exp(-z_h t) + 2A_s\exp(-\Gamma_s t) \times[\cos(\omega_s t) + b\sin(\omega_s t)]. \tag{9}$$

Although the Eq. (8) contains six parameters, they are all functions of the three independent parameters given in Eq. (5). Therefore, the normalized dynamic structure factor is the function of the three independent adjustable parameters for which the low-k limits are known exactly.

One can also cast the TEE model in the form of a continued fraction expansion [27],

$$S(k,z) = \left[z + \frac{f_{un}^2(k)}{z + z_u(k) + \dfrac{f_{uT}(k)}{z+z_T(k)}}\right]^{-1}. \tag{10}$$

From this, the second-order memory function of the correlation function of the density fluctuation is given as:

$$K_L(k,z) = z_u(k) + \frac{f_{uT}(k)}{z+z_T(k)}, \tag{11}$$

with a Marlkovian viscosity term $z_u(k)$ and a thermal fluctuation term having the finite decay time $z_T(k)$ [27]. From Eq. (10), we can also see two special cases of the TEE model.

When $f_{uT}(k) = 0$, the model becomes a damped harmonic oscillation (DHO) model [8,22], where the amplitude of the central peak of $S(k,\omega)$ is zero, the side peaks represented by the last two terms in Eq. (8) can be rewritten as:

$$S(k,\omega)/S(k) = \frac{1}{\pi}\frac{f_{un}^2(k)z_u(k)}{[\omega^2 - f_{un}^2(k)]^2 + [\omega z_u(k)]^2}. \tag{12}$$

When $z_u(k) = 0$, the second-order memory function only consists of one Lorentzian form with the decay time $z_T(k)$, which is the so-called viscoelastic model [27,28].

To fit the IXS data, we use the three adjustable parameters in the matrix [Eq. (5)]. Figure 4 shows the IXS spectra at $T = 273$ K [Fig. 4(a)], $T = 294$ K [Fig. 4(b)] at different k values together with the model calculations (solid lines) which are already convoluted with the energy resolution function. Figure 5 shows the three extracted fitting parameters of TEE model and the input static structure factor $S(k)$ [5].

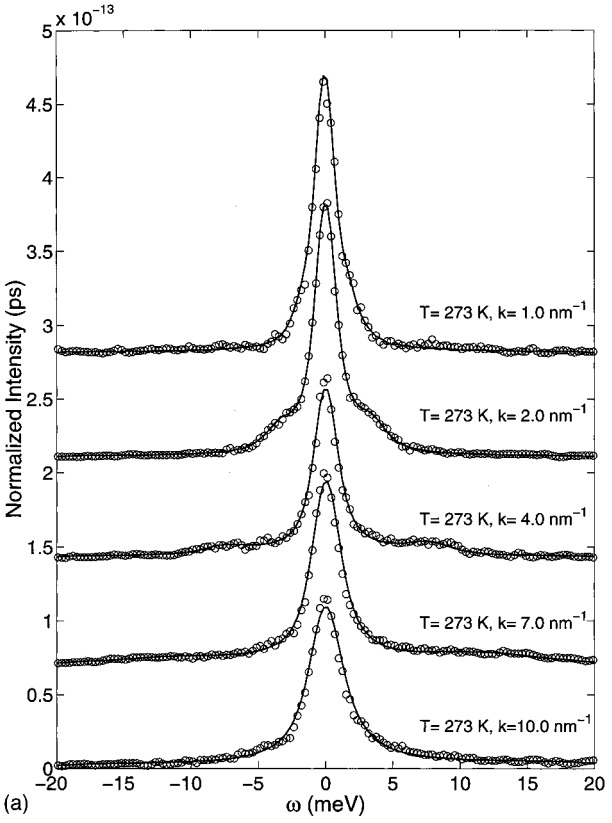

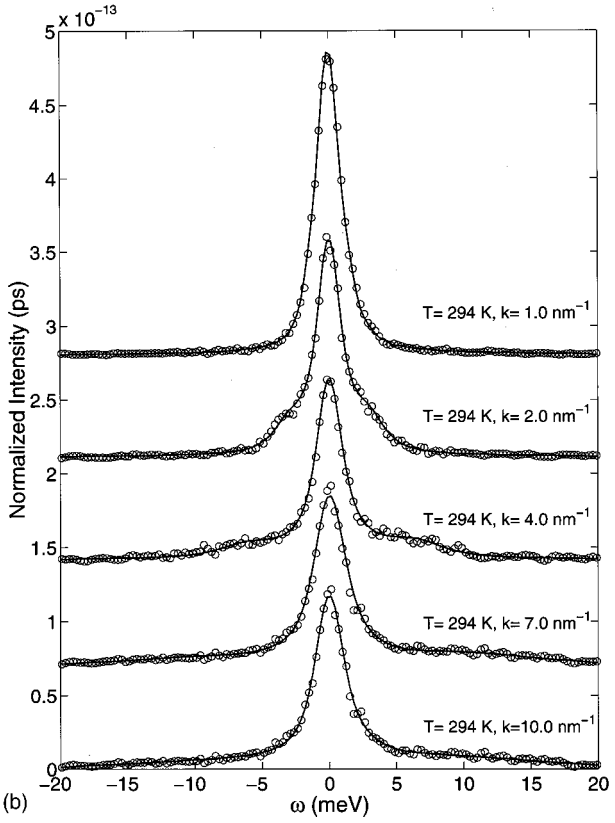

FIG. 4. (a) The IXS spectra of H_2O at $T=273\,K$ taken at the indicated k values. The experimental data (open circle) are superimposed to the fit (solid line) by the TEF model as explained in the text. (b) The IXS spectra of H_2O at $T=294\,K$ taken at the indicated k values. The experimental data (open circle) are superimposed to the fit (solid line) by the TEE model as explained in the text.

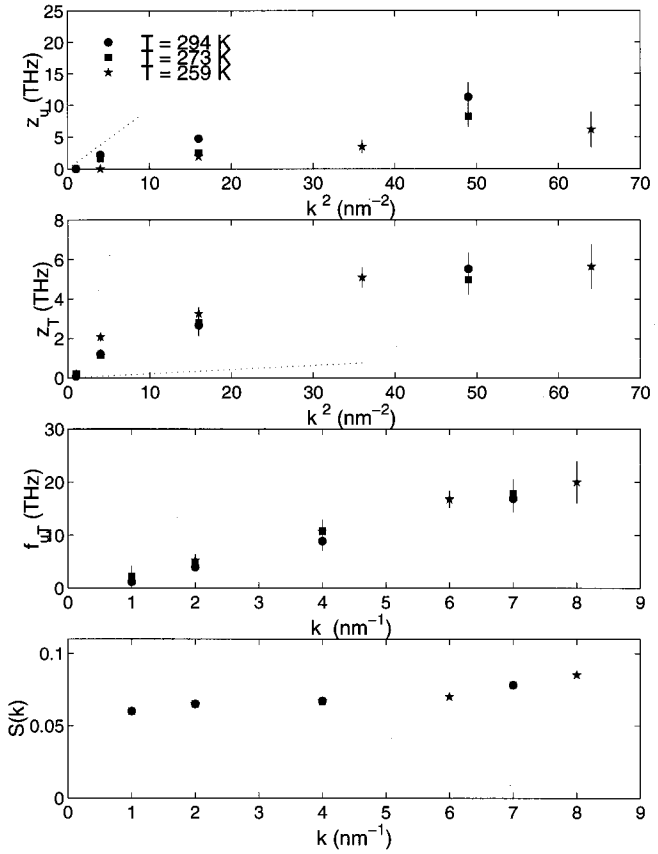

FIG. 5. The extracted fitting parameters from IXS spectra by Three Effective Eigenmode model at indicated temperatures, plotted together with the input static structure factor. The dotted lines are the expected hydrodynamic behaviors.

IV. SOUND PROPAGATION AND RELAXATION RATE

The sound speed and sound damping are well defined in the Brillouin light scattering [29,30], where the sound speed is the position of the side peak divided by the k value and the sound damping is the width of the side peak. Table II lists the physical properties of water, including the quantities to determine the low-frequency sound speed and damping. In the case of IXS and INS, where k value becomes comparable with the inverse of the typical inter-molecular distance, the above hydrodynamic behavior is replaced by kinetic effects of molecular collisions manifesting through the merging of

TABLE II. Physical properties of H_2O at 1 atm, 273 K [29].

Density ρ (kg/m^3)	1.0
Specific Heat Ratio $\gamma=c_p/c_v$	~1.0
Isothermal compressibility K_T (10^{-6} bar^{-1})	52.24
Adiabatic Sound Speed $c_s=(\gamma/\rho K_T)^{1/2}$ (m/s)	1380
Shear Viscosity η (10 kg m^{-1} s^{-1})	18.284
Ratio of the bulk to shear viscosity ζ/η	1.90
Longitudinal viscosity $\phi=[(4/3)\eta+\zeta]/\rho$ (10^{-3} cm s^{-1})	59.1
Specific heat at constant pressure c_p (kJ kg^{-1} K^{-1})*	4.22
Thermal conductivity λ (10^{-3} W m^{-1} K^{-1})*	561.1
Thermal diffusivity $D_T=\lambda/\rho c_p$ (10^{-3} cm^2 s^{-1})	1.33

*From Ref. [31].

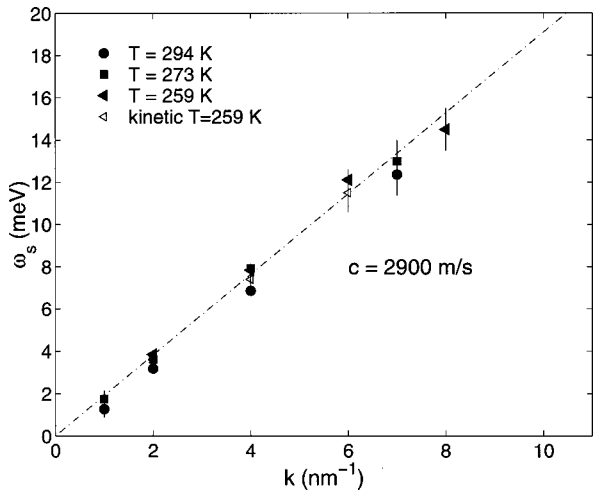

FIG. 6. The dispersion curve of H_2O extracted from IXS spectra at the indicated temperatures. The solid symbols denote ω_s from the TEE model, and the open symbols are from the dynamic cage (kinetic) model. The dash-dotted line represents a dispersion curve with a sound speed $c=2900$ m/s.

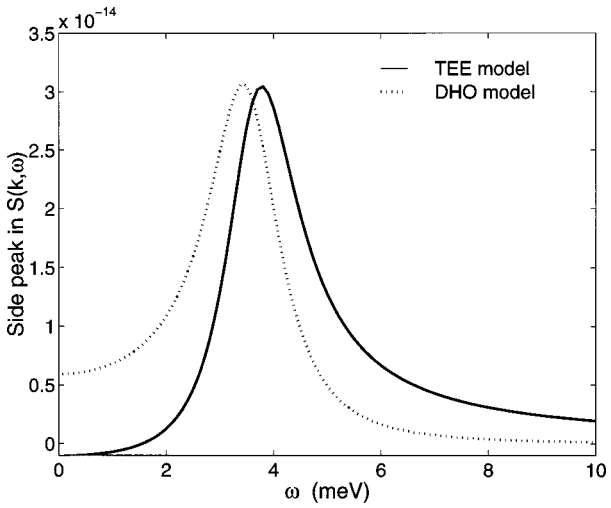

FIG. 7. The side peaks calculated by DHO model (dotted line) and TEE model (solid line). The parameters [including ω_s, Γ_s, b in Eq. (8)] in the TEE model are taken from the best fitting of the IXS spectra of water at $k=2\ \mathrm{nm}^{-1}$ and $T=273$ K. For the DHO model [Eq. (13)], $\Omega=\omega_s$, $\Gamma=2\Gamma_s$, the amplitude is arbitrary.

the Raleigh-Brillouin triplets into one nearly Gaussian line in most of the measured scattering wave vector range. In fact, even at the lowest magnitude of k measured, the triplet exhibits a huge peak at the center with two weak shoulders at the side (see Figs. 2 and 4). These side shoulders are the evidence of the collective excitations. As an example in Fig. 4(a), at $k=2.0\ \mathrm{nm}^{-1}$ a broad inelastic shoulder occurs at around 3.7 ± 0.5 meV, which gives the sound velocity around 2810 ± 400 m/s. As k becomes larger, the increasing damping of the sound mode makes the sound excitations less visible. In order to get a reliable sound speed, the model calculation is needed. At $k=10.0\ \mathrm{nm}^{-1}$, the sound mode almost merges into the long tail of the quasielastic peak.

Using the two models described in the Secs. II and III, we successfully extracted the sound speed and the sound damping. Figure 6 shows the dispersion curve extracted from IXS spectra. The sound excitation frequencies (solid symbols) in this figure are defined as the imaginary part of the complex eigenvalue of the hydrodynamiclike matrix given in Eq. (5), which is also the positions of the two side peaks in $S(k,\omega)$ defined as the last two terms of r.h.s. in Eq. (8). In this figure, we also show the sound excitation frequencies extracted from the dynamic cage model (open symbols), which are the side peak positions of the QTRT contribution. Because the side peaks in the QTRT contribution become difficult to be identified at larger k values, we can only extract three lowest k values ($k=2,4,6\ \mathrm{nm}^{-1}$) with the error bars indicating the uncertainty to determine the peak positions. The dispersion curves extracted from the two models agree quite well, giving the sound speed $c=2900\pm300$ m/s, which is about twice the adiabatic sound speed at low frequency. This value of the high frequency sound speed is slightly smaller than the values given in the Refs. [8] and [9]. The reason for this disagreement is because they are extracted using different models. In the Refs. [4], [8] and [9], the side peaks are described by the DHO model given as,

$$S(k,\omega)/S(k)=\frac{1}{\pi}\frac{\Omega\Gamma^2}{(\omega^2-\Omega^2)^2+(\omega\Gamma)^2}. \qquad (13)$$

In the TEE model the side peaks are modeled by a hydrodynamic-like formalism [the last two terms in the r.h.s. of Eq. (8)]. Figure 7 shows the difference between these two descriptions. One can see that even though the two models use the same value of the peak position parameter, the TEE mode produces a side peak always at the right-hand side of one produced by DHO model. That is to say, to generate a same side peak, the DHO model must have a larger value of Ω.

Figure 8 shows the sound damping at different k and temperatures. The sound damping Γ_s in TEE model is defined as the real part of the complex eigenvalue of the hydrodynamiclike matrix [Eq. (5)]. Also shown is the line width of the side peak by INS of liquid D_2O at room temperature [4]. They both demonstrate a similar variation proportional to k^2

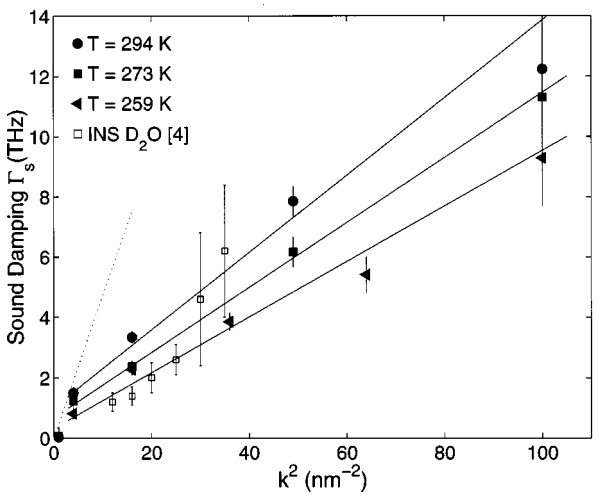

FIG. 8. The sound damping plotted against k^2 extracted from IXS spectra. The solid symbols refer to Γ_s from the TEE model, the open symbols to side peak line width from the Ref. [4], the dotted line to the hydrodynamic extrapolation at $T=273$ K, and the solid straight line is guided by the eye.

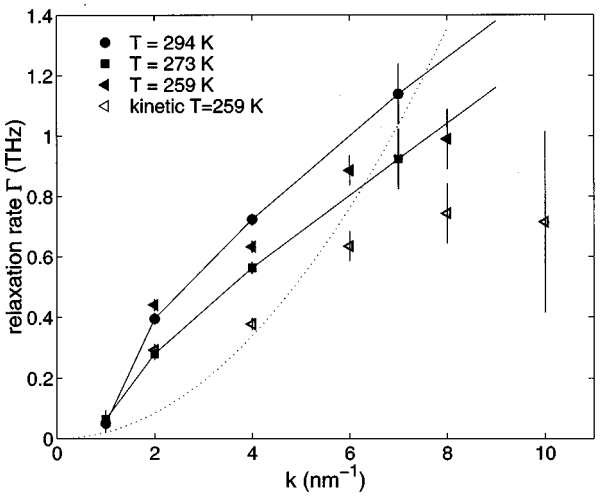

FIG. 9. The relaxation rate of the central peak extracted from IXS spectra. The solid symbols refer to Γ from the TEE model, the open symbols to the average relaxation rate of the stretched exponential in dynamic cage model. The dotted line is the hydrodynamic extrapolation at $T=273$ K. The solid lines are the direct connections of the symbols.

(except the two data of highest k in Ref. [4] with large error bars), and much smaller than the hydrodynamic extrapolation to this k range. The sound damping from the IXS data also shows a temperature dependent behavior: as temperature decreases, the sound excitation peak becomes sharper.

The relaxation rate represented by the width of the quasielastic peak is difficult to determine because the resolution function of IXS spectrometer is much wider than the true width of the central peak of $S(k,\omega)$. In this case, the sensitive part of $S(k,\omega)$ in fitting process is not the shape of the central peak, but the width, height of the central peak and the contributions of the side peak to the low-frequency part. In the dynamic cage model, we fit the central peak as the Fourier transform of the stretched exponential, where in the TEE model, we fit with the Lorentzian function. Figure 9 shows the relaxation rate extracted from these two models. In the TEE model, the relaxation rate is defined to be $\Gamma(=z_h)$, the real eigenvalue of the matrix in Eq. (5). In the dynamic cage model, the relaxation rate is the average relaxation rate of stretched exponential, which is

$$\Gamma=\frac{1}{\tau}=\frac{\beta}{\tau G(1/\beta)}, \tag{14}$$

with $G(x)$ the gamma function. One can easily verify that as $\beta=1$, this definition becomes the spectral width of the exponential function and is equivalent to the definition in the TEE model. From Fig. 9, one can see that the central peak becomes wider as k increases and temperature increases in the normal liquid region (T is larger than 273 K). The relaxation rate at $T=259$ K displays a different variation, which may be related to the extra pressure applied to the sample. The different values at $T=259$ K obtained from the TEE model and the dynamic cage model are due to the different contributions to the low-frequency part by the inelastic part.

V. DISCUSSION AND CONCLUSION

We have analyzed a set of IXS spectra of low temperature water using two different models: the dynamic cage model and TEE model. From these analysis, we are able to obtain the Debye-Waller factor and the cage relaxation time at the lowest temperature ($T=259$ K), and the high frequency sound dispersion relation, the sound damping and the relaxation rate associated with the quasi elastic peak. The Debye-Waller factor in the lowest temperature is consistent with our previous study of the SPC/E water at supercooled state [12]. We have shown the significance of the relative proportion and mutual interaction between the quasi elastic peak and inelastic peaks in the model descriptions. In order to extract reliable values of physical quantities, it is important to have a correct theory for the description of the triplet, not just a phenomenological fitting function.

We note that the two models we used for data analysis can be cast into one similar form: a central peak plus two symmetric side peaks. For the dynamic cage model, the central peak is the Fourier transform of the stretched exponential and the side peak is mainly due to the contribution of the modified QTRT kinetic model. For the TEE model, the central peak is the Fourier transform of the exponential function and the side peak is a hydrodynamiclike function. While the TEE model well describes the IXS spectra for all three temperatures, the dynamic cage model is only used to fit the lowest temperature data. We also note from a recent MD simulation [12,13] that in the supercooled water, the intermediate scattering (ISF) function exhibits a well-separated two-step decay and the long-time α relaxation is a stretched exponential. This MD generated ISF, without being smeared by a resolution function, is well described by the dynamic cage model [12]. But it can not be fitted with the TEE model which fails to generate a stretched exponential decay. This fact indicates that the TEE model is only suitable for the normal fluids where the cage life time (relaxation time) is not long enough for the cage effect to become dominant in the dynamic process. But the dynamic cage model, which successfully incorporates both the appropriate short-time collisional dynamics and a long-time structural relaxation in supercooled liquids where the cage effect is dominant, is suitable for describing dynamics in supercooled liquids.

ACKNOWLEDGMENTS

We are grateful to Dr. I. M. de Schepper for an extensive communication in which he described the uses of the three effective eigenmode theory to us. The part of research done at MIT is supported by a grant from Materials Research Division of the U.S. DOE.

APPENDIX

Here, we derive the three effective eigenmode model based on the method described in Ref. [19]. We consider the dynamic correlation functions

$$F_{\alpha\beta}(k,z)=\left\langle b_\alpha^*(k)\frac{1}{z-L}b_\beta(k)\right\rangle \tag{A1}$$

where the bracket $\langle\rangle$ indicates an equilibrium average over a canonical ensemble of N particles, the star denotes complex conjugation, L is the Liouville operator of the system given by

$$L=\sum_{i=1}^{N}\left[\mathbf{v}_i\cdot\frac{\partial}{\partial\mathbf{r}_i}-\frac{1}{m}\sum_{i\neq j}\frac{\partial\phi_{ij}}{\partial\mathbf{r}_{ij}}\cdot\frac{\partial}{\partial\mathbf{v}_i}\right], \tag{A2}$$

and $b_\alpha(k)$ are the microscopic fluctuation with the first three conserved quantities defined as,

$$b_1(k)=\frac{1}{\sqrt{NS(k)}}\sum_{j=1}^{N}e^{-ik\cdot r_j} \tag{A3}$$

is the microscopic density fluctuation;

$$b_2(k)=\frac{1}{\sqrt{N}}\sum_{j=1}^{N}\frac{\mathbf{k}\cdot\mathbf{v}_j}{kv_0}e^{-ik\cdot r_j} \tag{A4}$$

is the microscopic longitudinal velocity fluctuation with $v_0=(k_BT/m)^{1/2}$ the thermal velocity; and

$$b_3(k)=\frac{1}{\sqrt{N}}\sum_{j=1}^{N}\frac{3-mv_j^2/(k_BT)}{\sqrt{6}}e^{-ik\cdot r_j} \tag{A5}$$

is the microscopic temperature fluctuation. One can also define the microscopic dynamic quantities $b_\alpha(k)$ at $\alpha>3$, so that they are orthonormal including the above defined hydrodynamic conserved quantities [21]

$$\langle b_\alpha^*(k)b_\beta(k)\rangle=\delta_{\alpha\beta} \tag{A6}$$

and complete,

$$\sum_\alpha|b_\alpha(k)\rangle\langle b_\alpha(k)|=\mathbf{I}. \tag{A7}$$

The Eq. (A1) can be rewritten as

$$F_{\alpha\beta}(k,z)=\langle b_\alpha(k)|b_\beta(k,z)\rangle \tag{A8}$$

with

$$|b_\beta(k,z)\rangle=\frac{1}{z-L}|b_\beta(k)\rangle, \tag{A9}$$

so that

$$z|b_\beta(k,z)\rangle=L|b_\beta(k,z)\rangle+|b_\beta(k)\rangle. \tag{A10}$$

Then after multiplying $\langle b_\alpha^*(k)|$ to the Eq. (A10) and using Eqs. (A7) and (A8) we get:

$$zF_{\alpha\beta}(k,z)=\sum_\gamma L_{\alpha\gamma}^{\infty}(k)F_{\gamma\beta}(k,z)+\delta_{\alpha\beta}, \tag{A11}$$

where the element of the infinite symmetric matrix is

$$L_{\alpha\beta}^{\infty}(k)=\langle b_\alpha(k)|L|b_\beta(k)\rangle. \tag{A12}$$

In order to contract the infinite matrix equation of Eq. (A10) to a 3×3 matrix equation, we can decompose an infinite matrix A into four blocks as:

$$\vec{\vec{A}}=\lim_{M\to\infty}\begin{bmatrix}\vec{\vec{A}}_{33} & \vec{\vec{A}}_{3M}\\ \vec{\vec{A}}_{M3} & \vec{\vec{A}}_{MM}\end{bmatrix}, \tag{A13}$$

where $\vec{\vec{A}}_{33},\vec{\vec{A}}_{3M},\vec{\vec{A}}_{M3},\vec{\vec{A}}_{MM}$ represents the matrix of $3\times3,3\times M,M\times3,M\times M$, respectively. One then can write out the equation for the correlation function $\vec{\vec{G}}_{33}(k,z),\vec{\vec{G}}_{M3}(k,z)$ from Eq. (A11) as

$$z\vec{\vec{G}}_{33}(k,z)=\vec{\vec{L}}_{33}(k)\vec{\vec{G}}_{33}(k,z)+\vec{\vec{L}}_{3M}(k)\vec{\vec{G}}_{M3}(k,z)+\vec{\vec{I}}_{33} \tag{A14}$$

$$z\vec{\vec{G}}_{M3}(k,z)=\vec{\vec{L}}_{M3}(k)\vec{\vec{G}}_{33}(k,z)+\vec{\vec{L}}_{MM}(k)\vec{\vec{G}}_{M3}(k,z). \tag{A15}$$

The correlation function $\vec{\vec{G}}_{M3}(k,z)$ can be solved out from Eq. (A14), and inserted into Eq. (A13) one gets

$$z\vec{\vec{G}}_{33}(k,z)=\vec{\vec{H}}_{33}(k,z)\vec{\vec{G}}_{33}(k,z)+\vec{\vec{I}}_{33}, \tag{A16}$$

with a z-dependent 3×3 matrix

$$\vec{\vec{H}}_{33}(k,z)=\vec{\vec{L}}_{33}(k)+\vec{\vec{L}}_{3M}(k)[z\vec{\vec{I}}_{MM}-\vec{\vec{L}}_{MM}(k)]^{-1}\vec{\vec{L}}_{M3}(k). \tag{A17}$$

From the fact

$$Lb_1(k)=\frac{-ikv_0}{\sqrt{S(k)}}b_2(k) \tag{A18}$$

one can get that the elements of the first column and the first row of the matrix $\vec{\vec{L}}^{\infty}(k)$ are all zero, except the two elements

$$L_{21}^{\infty}(k)=L_{12}^{\infty}(k)=-if_{un}(k)=\frac{-ikv_0}{\sqrt{S(k)}}. \tag{A19}$$

This makes the 3×3 matrix $\vec{\vec{H}}_{33}(k,z)$ containing only three unknown quantities: $H_{22}(k,z)$, $H_{23}(k,z)$ $[=H_{23}(k,z)]$, $H_{33}(k,z)$. The z dependence of the elements comes from the z dependence of the second term of the Eq. (A14), which is the z dependence of the correlation function of the three hydrodynamic fluctuation with other dynamic quantities ($\alpha>3$). When the time decay of the correlation function $G_{\alpha\beta}(k,t)(\alpha<3,\beta>3)$ is much faster then the decay of the correlation function $G_{\alpha\beta}(k,t)(\alpha<3,\beta<3)$, which means the considered correlation spectra $G_{\alpha\beta}(k,z)(\alpha<3,\beta<3)$ are much closer to low-frequency region, one can introduce an approximation by setting the $z=0$ at the left-hand side of the Eq. (A15) and hence the z-dependent matrix $\vec{\vec{H}}_{33}(k,z)$ is replaced by the matrix $H(k)=\vec{\vec{H}}_{33}(k,z=0)$.

One can show that the above derivation is equivalent to the projection formalism used to derive a 5×5 effective eignemode description in Ref. [1].

[1] I. M. de Schepper, E. G. D. Cohen, C. Bruin, J. C. van Rijs, W. Montfrooij, and L. A. de Graaf, Phys. Rev. A **38**, 271 (1988).
[2] G. Ruocco and F. Sette, J. Phys.: Condens. Matter **11**, R259 (1999).
[3] A. Rahman, and F. H. Stillinger, Phys. Rev. A **10**, 368 (1974).
[4] J. Teixeira, M. C. Bellissent-Funel, S. H. Chen, and B. Dorner, Phys. Rev. Lett. **54**, 2681 (1985).
[5] F. Sciortino and S. Sastry, J. Chem. Phys. **100**, 3881 (1994).
[6] U. Balucani, G. Ruocco, A. Torcini, and R. Vallauri, Phys. Rev. E **47**, 1677 (1993).
[7] F. J. Bermejo, M. Alvarez, S. M. Bennington, and R. Vallauri, Phys. Rev. E **51**, 2250 (1995).
[8] F. Sette, G. Ruocco, M. Krisch, U. Bergmann, C. Masciovecchio, V. Mazzacurati, G. Signorelli, and R. Verbeni, Phys. Rev. Lett. **75**, 850 (1995).
[9] F. Sette, G. Ruocco, M. Krisch, C. Masciovecchio, R. Verbeni, and U. Bergmann, Phys. Rev. Lett. **77**, 83 (1996).
[10] A. Cunsolo, G. Ruocco, F. Sette, C. Masciovecchio, A. Mermet, G. Monaco, M. Sampoli, and R. Verbeni, Phys. Rev. Lett. **82**, 775 (1999).
[11] R. Verbeni, F. Sette, M. Krisch, U. Bergmann, B. Gorges, C. Halcoussis, K. Martel, C. Masciovecchio, J. F. Ribois, G. Gruocco, and H. Sinn, J. Synchrotron Radiat. **3**, 62 (1996); C. Masciovecchio, U. Bergmann, M. Krisch, G. Ruocco, F. Sette, and R. Verbeni, Nucl. Instrum. Methods Phys. Res. B **111**, 181 (1996).
[12] C. Y. Liao, F. Sciortino, and S. H. Chen, Phys. Rev. E **60**, 6776 (1999).
[13] F. Sciortino, L. Fabbian, S. H. Chen, and P. Tartaglia, Phys. Rev. E **56**, 5397 (1997).
[14] P. M. Furtado, G. F. Mazenko, and S. Yip, Phys. Rev. A **13**, 1641 (1976).
[15] J. P. Boon and S. Yip, *Molecular Hydrodynamics* (McGraw-Hill, New York, 1980).
[16] S. Yip, W. E. Alley, and B. J. Alder, J. Stat. Phys. **27**, 201 (1982).
[17] K. Toukan, S. H. Chen, and S. Yip, Mol. Phys. **55**, 1421 (1985).
[18] J. M. Zanotti, M. C. Bellissent-Funel, and S. H. Chen, Phys. Rev. E **59**, 3084 (1999).
[19] B. Kamgar-Parsi, E. G. D. Cohen, and I. M. de Schepper, Phys. Rev. A **35**, 4781 (1987).
[20] W. E. Alley, and B. J. Alder, Phys. Rev. A **27**, 3158 (1983).
[21] E. G. D. Cohen, I. M. de Schepper, and M. J. Zuilhof, Physica B **127**, 282 (1984).
[22] W. Montfrooij, E. C. Svensson, I. M. de Schepper, and E. G. D. Cohen, J. Low Temp. Phys. **105**, 149 (1996).
[23] R. Zwanzig, in *Lectures in Theoretical Physics*, edited by W. Brittin (Wiley-Interscience, New York, 1961), Vol. 3, pp. 106–141.
[24] H. Mori, Prog. Theor. Phys. **33**, 423 (1965).
[25] E. D. G. Cohen, and I. M. de Schepper, Nuovo Cimento **12**, 521 (1990).
[26] U. Bafile, P. Verkerk, F. Barocchi, L. A. de Graaf, J.-B. Suck, and H. Mutka, Phys. Rev. Lett. **65**, 2394 (1990).
[27] U. Balucani, and M. Zoppi, *Dynamics of the Liquid State* (Clarendon, Oxford, 1994).
[28] I. M. de Schepper (private communication).
[29] J. Rouch, C. C. Lai, and S. H. Chen, J. Chem. Phys. **66**, 5031 (1977).
[30] J. Rouch, C. C. Lai, and S. H. Chen, J. Chem. Phys. **65**, 4016 (1976).
[31] W. W. A. Kruse, *Properties of Water and Steam* (Springer-Verlag, Berlin, 1998).